AFRL-OSR-VA-TR-2013-0126

University Capstone Project: Enhanced Initiation Techniques for Thermochemical Energy Conversion

Frederick L. Dryer

Princeton University

March 2013
Final Report

AIR FORCE RESEARCH LABORATORY
AF OFFICE OF SCIENTIFIC RESEARCH (AFOSR)
ARLINGTON, VIRGINIA 22203
AIR FORCE MATERIEL COMMAND

REPORT DOCUMENTATION PAGE

Form Approved
OMB No. 0704-0188

PLEASE DO NOT RETURN YOUR FORM TO THE ABOVE ORGANIZATION.

1. REPORT DATE *(DD-MM-YYYY)*	2. REPORT TYPE	3. DATES COVERED *(From - To)*
31-12-2012	FINAL	30-09-2010 - 29-09-2012

4. TITLE AND SUBTITLE

University Capstone Project: Enhanced Initiation Techniques for Thermochemical Energy Conversion

5a. CONTRACT NUMBER

5b. GRANT NUMBER
FA9550-10-1-0552

5c. PROGRAM ELEMENT NUMBER

6. AUTHOR(S)
Ju, Yiguang
Dryer, Frederick L.

5d. PROJECT NUMBER

5e. TASK NUMBER

5f. WORK UNIT NUMBER

7. PERFORMING ORGANIZATION NAME(S) AND ADDRESS(ES)
Princeton University
4 New South Bldg.,
Princeton, NJ 08544

8. PERFORMING ORGANIZATION REPORT NUMBER

9. SPONSORING/MONITORING AGENCY NAME(S) AND ADDRESS(ES)
AFOSR
875 N Randolph St
Arlington, VA 22203

10. SPONSOR/MONITOR'S ACRONYM(S)

11. SPONSOR/MONITOR'S REPORT NUMBER(S)
AFRL-OSR-VA-TR-2013-0126

12. DISTRIBUTION/AVAILABILITY STATEMENT
Distribution A: Approved for public release

13. SUPPLEMENTARY NOTES

14. ABSTRACT

A microwave-assisted spark plug and a nano-second pulsed spark plug were developed to enhance ignition and combustion efficiency for a small scale internal combustion engine and a pulse detonation engine. An engine test platform was developed to measure engine torque and pressure quantitatively. The experimental results demonstrated the superior characteristics of engine performance using these new ignition systems. The experimental tests of the microwave-enhanced spark ignition for two small scale engines (Fuji BF-34EI 34 cc engine) showed that the microwave-assisted ignition system was able to broaden the engine lean operational limits by more than 20%. Moreover, a significant increase of the maximum engine pressure was observed. The nanosecond-pulsed device was tested in collaboration with researchers at the AFRL in a pulse detonation engine at Wright-Paterson AFB. It was also found that the lean limit could be extended by the non-equilibrium plasma ignition system as compared to the conventional spark ignitor. Furthermore, the ignition time, which limits engine performance, could be reduced by up to 25%.

15. SUBJECT TERMS
Plasma-assisted combustion, Non-equilibrium plasma, Internal Combustion Engine ignition, Enhanced initiation

16. SECURITY CLASSIFICATION OF:			17. LIMITATION OF ABSTRACT	18. NUMBER OF PAGES	19a. NAME OF RESPONSIBLE PERSON
a. REPORT	b. ABSTRACT	c. THIS PAGE			Yiguang Ju
U	U	U	U		19b. TELEPHONE NUMBER *(Include area code)* 609-258-5644

Reset

Standard Form 298 (Rev. 8/98)
Prescribed by ANSI Std. Z39.18

Final Report

University Capstone Project:
Enhanced Initiation Techniques for Thermochemical Energy Conversion

Contract/Grant No. FA9550-10-1-0552
Research period: September 30, 2010 – September 29, 2012
Program Manager: Dr. Chiping Li, AFOSR/RSA

Principal Investigator: Prof. Yiguang Ju
Princeton University
Mechanical and Aerospace Engineering
School of Engineering and Applied Sciences
D-330 Engineering Quadrangle
Princeton University
Princeton, NJ 08544-5263

Phone: 609-258-5644
Email: yju@princeton.edu

Co-Investigators and Institutions:
Prof. Frederick L. Dryer Princeton University (PU)

December 31, 2012

Summary

A microwave-assisted spark plug and a nano-second pulsed spark plug were developed to enhance ignition and combustion efficiency for a small scale internal combustion engine and a pulse detonation engine. An engine test platform was developed to measure engine torque and pressure quantitatively. The experimental results demonstrated the superior characteristics of engine performance using these new ignition systems. The experimental tests of the microwave-enhanced spark ignition for two small scale engines (Fuji BF-34EI 34 cc engine) showed that the microwave-assisted ignition system was able to broaden the engine lean operational limits by more than 20%. Moreover, a significant increase of the maximum engine pressure was observed. The nanosecond-pulsed device was tested in collaboration with researchers at the AFRL in a pulse detonation engine at Wright-Paterson AFB. It was also found that the lean limit could be extended by the non-equilibrium plasma ignition system as compared to the conventional spark ignitor. Furthermore, the ignition time, which limits engine performance, could be reduced by up to 25%.

1. Introduction

Development of reliable ignition and lean burn technologies for small scale propulsion systems is challenging because of the increased heat and radical losses at large surface to volume ratios [1-4]. *Firstly*, for a small scale piston engine such as the 34 cc Fuji BF-34EI EIS 4-stroke engine, the engine stroke is only 28 mm. At a compression ratio of 10, for example, combustion at the top dead center has to occur at a compressed volume within a height of 2.8 mm, which is comparable to the quenching distance of a hydrocarbon fuel (2-4 mm) [5-7]. As a result, the lean burn region, engine efficiency, and fuel flexibility of such an engine are very constrained. *Secondly*, the conventional spark igniter is an equilibrium spark generated in a narrow gap (0.6-1 mm) between the electrodes. The large heat loss to the electrode reduces dramatically reduces the energy conversion efficiency, shortens the electrode longevity, and limits the maximum input of ignition energy. *Thirdly*, for large molecular hydrocarbon fuels, the mixture Lewis number is so large that the initial ignition kernel is affected strongly by the enthalpy loss due to flame stretch. *Finally*, a thermal plasma such as the conventional spark only provides heat and the electron temperature is too low (less than 1 eV) to produce any active radicals via electron impact dissociation to enhance ignition.

Therefore, the real technical challenges to address the enhancement of combustion in a small scale internal engine are the following:

- How can we produce active radicals/species more efficiently to enhance ignition?
- How can we break down the large fuel molecules to smaller ones to reduce the mixture Lewis number so that we can turn the enthalpy loss to enthalpy gain in the stretched ignition kernel?
- How can we understand better of the physical/chemical process of ignition initiation by plasma in a highly convective environment via optical imaging?
- Can we establish a standard test stand to assess the performance of ignition technologies quantitatively in a broad parametric range?

Recent progresses in non-equilibrium plasma assisted combustion [8-15] and microscale [1,2,3,6] combustion shed light on the development of reliable ignition and lean burn technologies for small scale propulsion systems. However, few efforts have been made to integrate the microscale combustion technology with non-equilibrium plasma assisted combustion for small scale power generation systems. Moreover, detailed kinetic and transport mechanisms of plasma-assisted enhancement on ignition and extinction remain unknown. Little quantitative experimental data are available to understand the kinetic processes that could lead to combustion enhancement and improved performance of a small scale engine, particularly for large hydrocarbon fuels.

The goal of this project was to develop: 1) new microwave assisted non-equilibrium plasma ignition systems using microwave and nano-second repetitive discharge approaches, 2) a platform to characterize the ignition and combustion properties of a small scale internal combustion engine, 3) a non-equilibrium plasma ignition system for efficient ignition in a pulse detonation engine. Specifically, the proposed research has the following three main thrusts:

I. Test a new microwave assisted ignition system,
II. Develop a new nano-second repetitive discharge ignition system,
III. Develop a platform to characterize power and combustion properties of a small scale internal combustion engine.
IV. Collaborate with AFRL to demonstrate the ignition enhancement in a PDE engine.

2. Experimental Studies of Microwave Assisted Engine Ignition

The goal of this study is to conduct preliminary tests on a non-equilibrium plasma-assisted ignition system as a means of operating small scale engines at leaner equivalence ratios over a wider load/speed range at improved specific fuel consumption, all of which would translate to improving UAV applications. An engine test platform which integrates the microwave ignition system with a small engine and dynamometer is established. The air/fuel (A/F) mass ratio is measured both by a combination of air and fuel flow measurements and by an exhaust gas A/F sensor, and the combustion chamber pressure is measured by an in-cylinder pressure transducer. To quantify the ignition enhancement, experiments are performed to measure engine stability ($COV_{imep,}$ Coefficient of variation of the indicated mean effective pressure) and specific fuel consumption (sfc) at lean conditions over a variety of engine load/speeds. In addition, the differences in the pressure profile for identical load/speed and A/F ratios are measured to quantify the differences in ignition development and flame propagation among the igniter used in this study.

2.1 Microwave-Enhanced Ignition System

Recently, Imagineering, Inc. has developed a novel microwave-enhanced spark plug for utilization in automobile engines [15, 16]. This device operates by channeling 2.45 GHz oscillating electrical energy from a commercial magnetron into a non-resistor spark plug, as shown in Fig. 1. The two electrodes of the spark plug act as a microwave antenna, and thus the

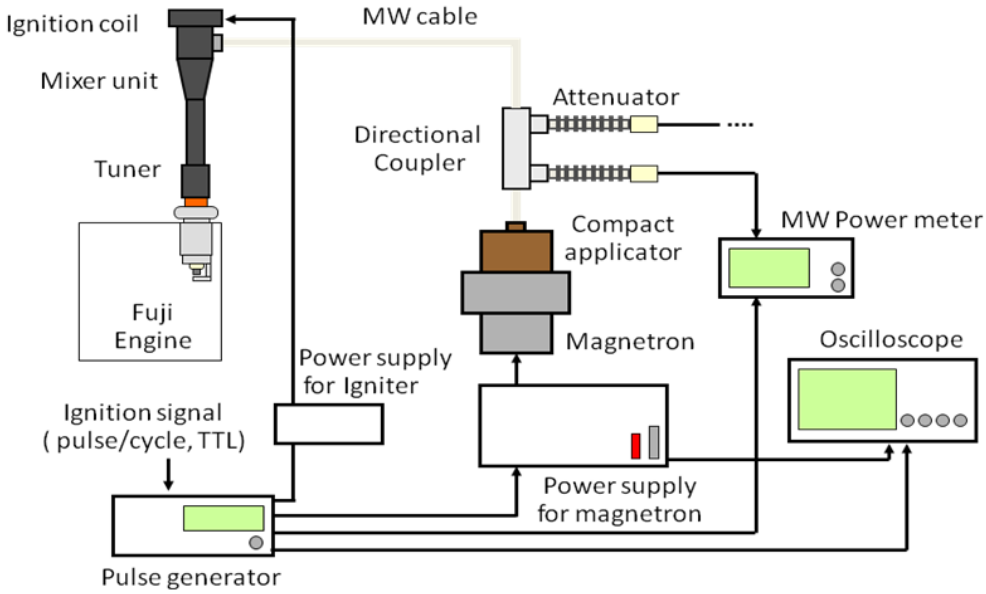

Figure 1 Diagram of microwave ignition system

geometry of the spark plug need not be altered from its original form. Once a spark is formed by a standard ignition coil, the microwave energy from the magnetron is absorbed by the electrons in the spark, which are raised to higher electronic states. These electrons collide with gas molecules and transfer their energy to create excited species. In a previous work investigating this ignition technology, the rotational temperature and N_2 density were measured by rotational Raman scattering in the region of the microwave discharge [16]. The prior study indicates that in the center of the 2.45 GHz microwave discharge in a 750 torr mixture of nitrogen and helium (700 torr nitrogen, 50 torr helium), the rotational temperature reached a maximum of roughly 1500 K, and at 4.5 mm from the center of the discharge the temperature reached as high as 750 K. It was found that the plasma remained in a non-equilibrium state for at least 1 ms after the discharge, as indicated by the temporally resolved temperature profile. This allows time for collisions of excited species with fuel, oxidizer, and diluents before the excited species relax into their equilibrium distribution, thus opening new combustion pathways. In addition, it was noted that the N_2 concentration was lower than expected for the initial conditions measured temperatures just after the discharge. This indicates that some of the N_2 may have been decomposed into atomic nitrogen, thus showing that this type of plasma can be effective at producing active radicals.

The microwave ignition system operates in burst mode, in which a series of pulses of 2.45 GHz microwave energy are delivered to the spark plug starting before and ending after the standard spark. The setup of the ignition system allows for control of spark timing, microwave pulse timing, and microwave burst duration. An encoder attached to the back side of the engine outputs a signal of one pulse per revolution of the crankshaft, set to occur at engine top dead center, which is fed into a BNC Model 575 pulse delay generator. Triggering off of the pulse occurring just after the exhaust stroke allows the delay generator to set a trigger signal anywhere during the compression or expansion stroke. The delayed signal is fed into an Elmos Model AWG50 waveform generator, as shown in Fig. 1. A trigger signal is sent to the igniter power supply for the initiation of the standard spark in the center electrode of the spark plug. The signal generator also outputs a series of pulses to the magnetron power supply lasting for a total of 2 ms for all experimental conditions. Each pulse is 4 μs long with 12 μs intervals between pulses. The magnetron output is channeled through a directional coupler and into an attenuation device for impedance matching, which is adjusted to minimize the reflected energy from the spark plug while in the engine. The reflected power is monitored by an Anritsu Model ML2488A power meter to ensure that the microwave signal is absorbed by the spark. A total of 750 mJ of electrical energy is delivered to the outer electrode of the spark plug, and 1/4 to 1/3 of that energy is reflected back. For comparison, the standard spark deposits ≤50 mJ of energy over a shorter time period. The signals output by the waveform generator and the magnetron power supply are monitored using a Tektronix Model DPO2024 oscilloscope, and the ignition timing is recorded for every experiment.

2.2 Small Engine Test Cells

Through a collaborative research between Princeton University and Imaging Engineering Inc., a small scale engine, Fuji Imvac Model BF-34EI, is coupled to a Fuji Electric dynamometer, and equipped with a 360 pulse per revolution encoder, an NTK air/fuel ratio sensor, a TSI air flow sensor, and a Kistler in cylinder pressure transducer for quantitative measurement and control of important engine parameters. This engine test cell is developed at

Imaging Engineering Inc. A picture of this setup is displayed in Fig. 2. The Fuji Imvac BF34-EI is a carbureted single cylinder, four-stroke engine with 34 cc of displacement (39 mm bore and 28 mm stroke length), weight of 2.6 kg, peak power output of 1.49 kW (2.0 hp) at 7,500 rpm, and peak torque of 1.96 Nm (46.5 lbft) at 5,000 rpm. Equivalence ratio of the intake charge can be adjusted via two knobs on the carburetor, one for high speed and one for low speed. All tests are performed using gasoline with an octane number of 90.1. The engine is coupled to a 7.5 kW (10 hp) Fuji Electric motor via a timing belt, allowing the engine to be driven and maintained at a constant rotational velocity.

The cylinder pressure is measured using a Kistler Type 6052 pressure transducer installed parallel to the spark plug in the engine head near the intake valve. The pressure signal is amplified using a Kistler Type 5064 signal amplifier. An encoder is mounted to the back side of the engine delivering 360 pulses per revolution and an additional signal of 1 pulse per revolution for triggering the ignition system. Both of these devices output to an Onosokki Type DS2000 engine monitoring system which is connected to a CPU for real time data monitoring and recording.

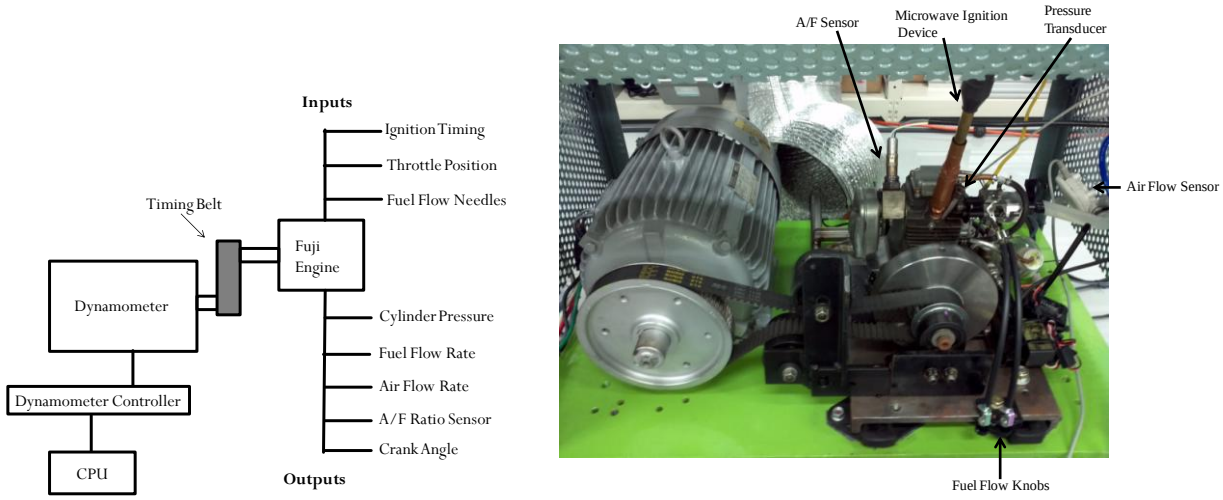

Figure 2 Diagram and picture of Imagineering engine test setup.

The air flow rate and temperature is monitored via a TSI Model 4021 mass flow meter. It is accurate to 2% of the reading or 0.05 standard L/min, whichever is greater, and has a response time of less than 4 msec. The fuel consumption is monitored by reading a graduated cylinder and taking time measurements every 5 mL at 5000 RPM and 2 mL at 2000 RPM. In addition, the A/F ratio is monitored with a Model ABM-10 NTK AF-Boost A/F ratio sensor installed in the exhaust port of the motor just before the muffler, which was found to have an absolute error of A/F = 1.2.

A similar test cell built at Princeton University is developed to integrate the same Fuji Imvac Model BF-34EI engine with a different dynamometer and sensor arrangement. Pictures of this setup can be found in Fig 3. The dynamometer is a Magtrol ED-715, which loads the engine

using a hysteresis brake, and is capable of controlling and measuring torque and rotational speed. Unlike the motor used by Imagineering, Inc., this dynamometer cannot be used to drive the engine. Instead, it is controlled by a Magtrol DSP6001 dynamometer controller which can be directly operated or operated from a computer using Magtrol MTest 5.0 software. Once the engine provides power to the dynamometer shaft, the controller can either set the torque or rotational speed to a given setting, using a PID control system to achieve the desired output. For

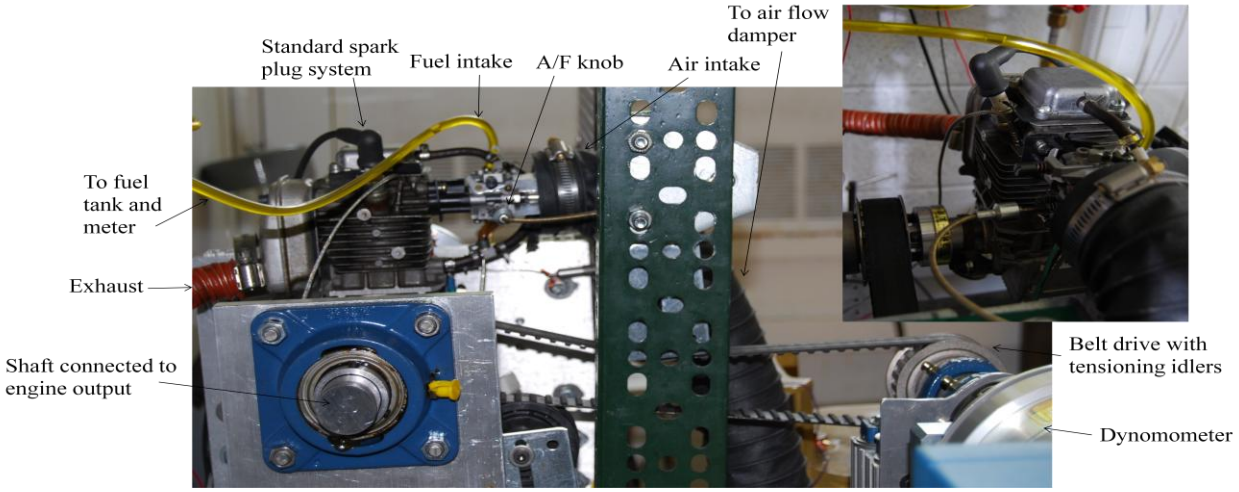

Figure 3 Princeton small engine test cell

these experiments, the dynamometer was always set to run the engine at a fixed rotation speed.

The engine output shaft (5/8" diameter) is coupled to the dynamometer using a belt and pulley assembly, which reduces the vibration transmitted to the dynamometer imposed by a direct connection. The output shaft of the engine is directly coupled via a rigid connection to a 1" diameter steel shaft which is set into two pillow block bearings. The pulley is fixed on the 1" shaft in between the engine and the bearings. This arrangement prevents bending of the output shaft due to the force imposed by the belt, as well as damps any vibrations from the engine. A common problem with this engine is that the crank shaft is not always perfectly manufactured, resulting in an eccentricity in the output shaft, which makes any flexible coupling to the dynamometer prone to vibration and eventual failure. In addition, the output shaft is easily bent, such that any asymmetric loading will worsen the wobble problem. The solution was to stiffly couple the engine output to the 1" shaft, thus not allowing any freedom for wobble. Another measure taken to reduce engine vibration was to attach a flywheel to the opposite side of the crankshaft. The flywheel was set on a shaft between two roller bearings and connected to the crank shaft via a flexible spider coupling. The throttle and choke of the engine are actuated by servo motors which are controlled via potentiometers integrated with a pulse width modulation circuit for adjusting the throttle position during engine start-up. For the tests conducted in this study, the throttle was always left at the wide-open (WOT) position. Equivalence ratio of the intake charge can be adjusted via two knobs on the carburetor, one for high speed adjustment, and one for low speed. The knobs can be adjusted during engine operation using a control cable fixed to the carburetor knob. To monitor the A/F ratio, the intake air flow rate is monitored via a TSI Model 4021 mass flow meter which outputs a digital signal for collection by the computer. It is accurate to within 2% of the reading or 0.05 standard L/min, whichever is greater, and has a

response time of less than 4 msec. To dampen the oscillations in the intake flow characteristic of IC engines, the engine intake is coupled to a 2.5" diameter hose leading to a 55 gallon drum. The drum has two ports, one connected to the engine hose and the other connected to the air flow meter. The air flow meter is free to pull atmospheric air through an air filter. Using this arrangement, there are no measurable oscillations in the flow rate measured by flow meter, thus the cycle-averaged air flow rate can be quantified. The fuel consumption rate is monitored by a Max Machinery Model 213 positive displacement flow meter which outputs 1000 pulses per cc of fuel consumed. The data from these two flow sensors is sent to a computer via a National Instruments Model 6210 DAQ board which has a sample rate of 250,000 samples per second. An in-house data collection program made in Labview is used to collect and store the data.

The cylinder pressure is measured using a Kistler 6052C Miniature Pressure Transducer installed parallel to the spark plug in the engine head near the intake valve. The signal is amplified with a Kistler 5010B Dual Model Amplifier and the signal can be outputted to either an oscilloscope for real time monitoring or into the test computer for data collection via the same Labview program previously mentioned. One Omega K-type thermocouple is currently used to monitor the temperature on the engine head to ensure overheating does not occur, and also to ensure steady-state operation has been achieved. A flow of compressed air is blown over the engine fins to provide convective cooling. Steady state operation of the engine can be achieved with head temperatures between 100-140 ºC.

Using the ignition device provided by the engine's original equipment manufacturer (OEM), ignition timing is controlled by reading a voltage signal from a Hall Effect sensor placed on the motor shaft, which gives the location of top dead center once every rotation. This signal is transmitted to the OEM electronic ignition module which computes the pre-programmed spark timing based on engine RPM and sends high-voltage energy to the spark plug. For use with the plasma ignition system, a different control scheme was implemented to allow the ignition timing to be varied at will. The crank angle is measured using an Encoder Products Company Model 260 quadrature encoder outputting 720 pulses per revolution on two channels, plus a third output signal of one pulse per revolution as a reference. The encoder is mounted to the dynamometer shaft, and is adjusted to give the reference signal at top dead center. The crank angle is thus known to within 0.5°. The signals from the encoder are sent via a National Instruments Model USB-6212 (16-Bit, 400,000 Samples/s DAQ board) to an in-house developed engine control system built in LabView. This program counts the pulses up to 720, and resets every time the reference signal is reached. In addition, this program can output a pulse via the same DAQ board at a user-defined crank angle. This output pulse is then sent to the ignition device.

In order to better control fuel properties and avoid batch-to-batch gasoline variations, a mixture of 90% iso-octane and 10% n-heptane (Octane number 90) were used for tests conducted at Princeton.

2.3 Experimental Results of Microwave Assisted Ignition in A Small Scale Engine

Motored engine tests were conducted at 2000 and 5000 rpm at wide open throttle (WOT). The maximum brake torque (MBT) timing for stoichiometric conditions was located and is listed in Table 1 as "Timing 1." The air/fuel mass ratio was varied from rich to increasingly lean conditions until the engine reached the lean misfire limit, which in this case was loosely judged to be the point at which the COV_{imep}>50%. When this limit occurred, the ignition timing was

advanced until the new MBT timing was established, and then the process of increasing the A/F ratio was continued. For these initial results, the MBT timing was changed 4 times at 2000 rpm and 3 times at 5000 rpm. Future tests mean to find the MBT timing at every A/F condition to truly establish the benefits of the microwave-assisted ignition system.

	Spark [C.A. ATDC]	MW Start [C.A. ATDC]	MW End [C.A. ATDC]
2000 rpm, Timing 1	17	-5	19
2000 rpm, Timing 2	-42	-69	-44
2000 rpm, Timing 3	-106	-128	-104
2000 rpm, Timing 4	-115	-141	-117
5000 rpm, Timing 1	-43	-96	-36
5000 rpm, Timing 2	-81	-148	-88
5000 rpm, Timing 3	-121	-188	-128

Table 1 Timing of spark and MW discharge

Each A/F ratio condition is tested with and without the use of the microwave-enhanced spark plug. The plotted data points represent the average pressure data for 263 engine cycles, maximum and minimum values of the A/F sensor readings over the period of data collection, one fuel consumption measurement of a fixed volume, and at least three engine cycles of air flow sensor data. It was found that A/F ratio measured by the AF-Boost meter and that measured by the combination of fuel flow rate and air flow rate data agree to within 5%, thus the experimental error is ±5% of the reported A/F value. The A/F sensor is limited to a maximum A/F ratio of 30, and fails to operate reliably when combustion is incomplete, so as the lean limit is approached it is necessary to rely only on the flow rate data.

Plotted in Fig. 4 is the COV_{imep} as a function of the A/F ratio. The microwave-assisted spark plug shows improvement to the COV_{imep} at most A/F ratio conditions, and again is most effective near the lean limit. Marked on this plot is the stable operating limit, defined as the point where engine operation becomes rough and unstable, and occurring at $COV_{imep} = 10\%$.[2] At 2000 rpm, the engine can operate within the stable operating limit consistently up to A/F ≈ 21 with the microwave-enhanced spark plug, while only rarely can an A/F ≥17 be reached with the standard spark. At MBT timing 3, the COV_{imep} is just outside of the stable operating limit at A/F = 28, which indicates that future tests may reveal more stable conditions at MBT timings set at A/F between 20 and 28. At 5000 rpm, the stable operating limit is definitively extended from A/F ≈ 17 for the standard plug to A/F ≈ 22 for the microwave-enhanced plug. In addition, in the range of A/F near stoichiometric conditions (A/F = 14.7) the COV_{imep} shows less unstable outliers with the microwave-assisted spark plug as compared to the standard spark case. As the timing is

advanced, the difference between the two plugs becomes more pronounced, until eventually combustion can only be achieved using the microwave-assisted spark plug. This result indicates that by using the microwave-assisted spark plug, the flame kernel development and flame propagation processes can be more fully completed using the microwave-assisted spark plug.

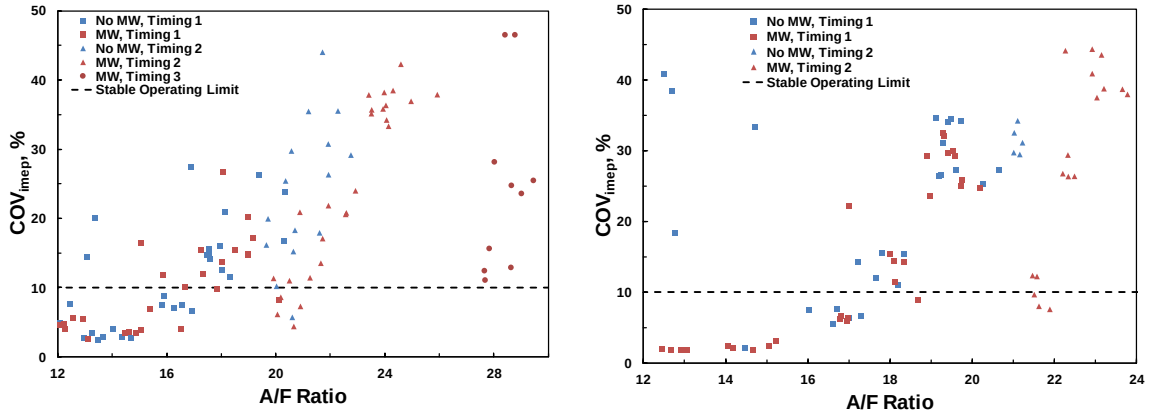

Figure 4 Coefficient of variation of the indicated mean effective pressure for standard and microwave-enhanced engine operation, showing the limit of stable operating conditions. Left: 2000 rpm, A/F = 23.5. Right: 5000 rpm, A/F = 22.2.

The imep as a function of A/F ratio is plotted in Fig. 5. At near stoichiometric (A/F~14.7) conditions, the engine outputs nearly the same imep using both spark plugs. However, in the range of A/F = 17-22, the microwave spark plug shows an average improvement in the imep of 9.8% at 2000 rpm and 6.1% at 5000 rpm. The microwave energy coupled into the spark for both cases only accounts for 2–2.25% of the total energy production, thus this increase in the imep is due to improvements in the ignition, kernel development, and flame propagation processes and their timing within the engine cycle. Figure 6 shows P-V diagrams just before the lean limit of normal spark plug operation for the 2000 and 5000 rpm cases, indicating the increased output of the microwave-spark plug at lean conditions for the same spark timing.

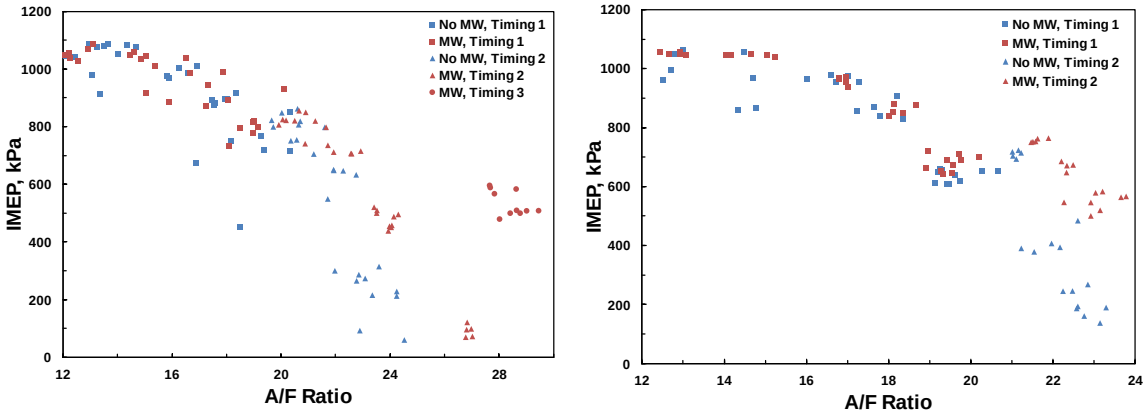

Figure 5 Indicated mean effective pressure as a function of air/fuel mass ratio. Left: 2000 rpm. Right: 5000 rpm

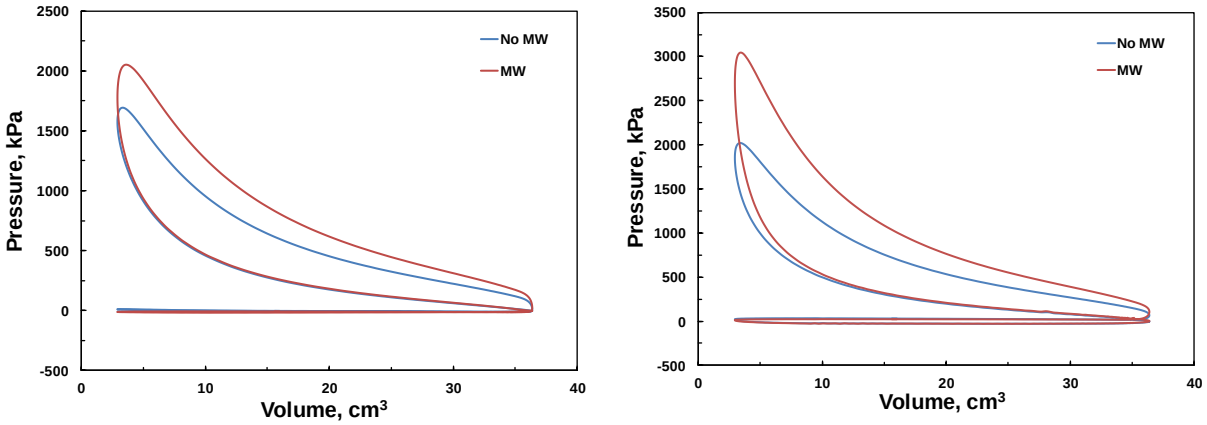

Figure 6 Pressure as a function of volume for standard and microwave-enhanced engine operation. Left: 2000 rpm, A/F = 23.5. Right: 5000 rpm, A/F = 22.2

The specific fuel consumption (sfc) is plotted as a function of A/F ratio in Fig. 7. For 2000 rpm, a minimum is reached between A/F = 17-20, and for 5000 rpm the minimum is between A/F =17-19. While there is little difference in the minimum sfc between the microwave-enhanced spark plug and the standard spark plug, it should be noted that in these A/F ranges, the COV_{imep} can be reduced by using the microwave-enhanced spark plug. Future tests which more completely explore the MBT timings for different A/F ratios will reveal the complete stable operating limits using the microwave-enhanced spark plug. However, these initial findings indicate that at lean conditions where the sfc is minimized, the improvement in the COV_{imep} is significant and should allow small engines to operate in the optimum range near A/F = 17-20.

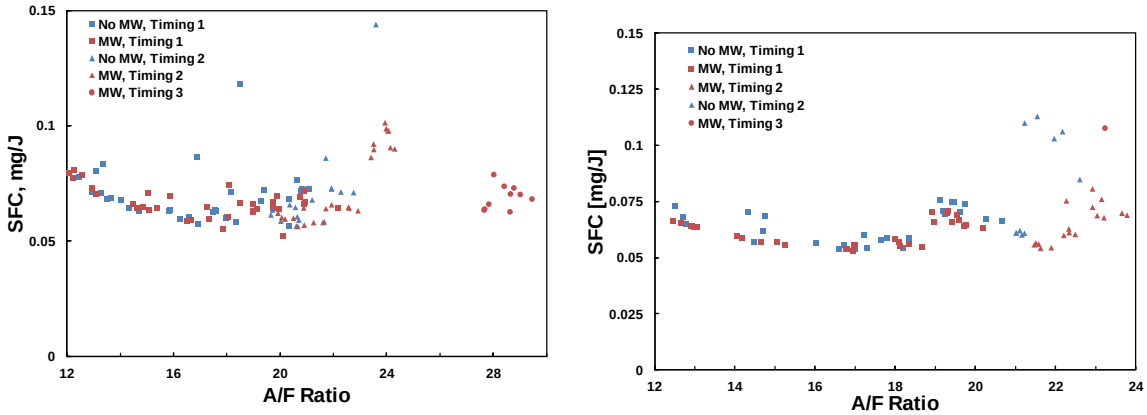

Figure 7 Specific fuel consumption as a function of A/F ratio. Left: 2000 rpm, A/F = 23.5. Right: 5000 rpm, A/F = 22.2

Another important parameter which was vastly improved by the plasma ignition system was the increase of maximum engine pressure. Plotted in Figure 8 is the maximum pressure as a function of crank angle. It is clear that the plasma igniter was capable of increasing the maximum pressure reached, as well as causing the maximum pressure to be achieved at closer to

top dead center as compared to the standard ignition system. This Figure best exemplifies the usefulness of plasma ignition. The top left branch of data points represents strong combustion events. It is clear that envelop of strong events is much larger with the plasma igniter.

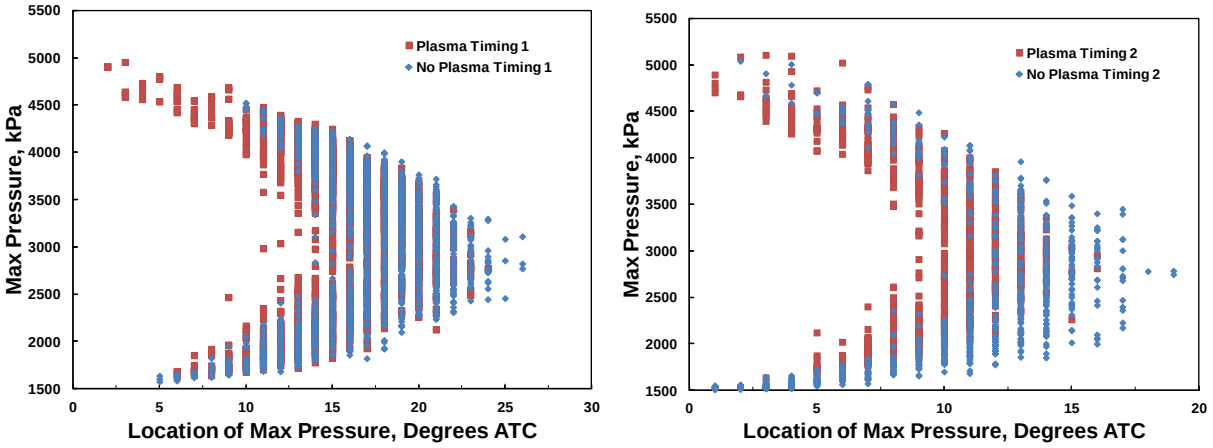

Figure 8 Max pressure as a function of crank angle. Left: 5000 rpm, Timing 1, Right: 5000 rpm, Timing 2.

3. Ignition Enhancement Demonstration in a Pulse Detonation Engine

3.1 Introduction

The development of ignition sources for combustion applications which operate near the conventional flammability limits and within restricted residence times is an active area of research centered on improving or enabling the operation of new engine designs. Ignition is one of the bottlenecks for technologies such as scramjets, gas turbine engines (relight and afterburner ignition), and pulsed detonation engines (PDEs) because of the limited residence times and low pressure conditions that exist within these systems. Many ignition studies in environments representative of the above mentioned systems have been focused on energy deposition using a variety of different techniques, but little effort has been placed on using high-frequency discharges. Recently, high-frequency nanosecond-pulsed discharges have been developed and applied for ignition studies in quiescent environments to show decreased ignition delay times with an increasing number of pulses [17]. The focus of this work was to extend the application of high-frequency nanosecond-pulsed discharges to a more relevant environment with some residence time restriction and levels of flow turbulence. This was accomplished through comparing the high-frequency nanosecond-pulsed discharge with a standard arc discharge on PDEs with measurements of ignition delay times as well as high-speed imaging of the ignition kernel growth.

PDEs were chosen for this investigation because they offered the easiest “plug-and-play” application while also allowing for the potential of significant ignition enhancement. For a PDE,

there are two basic methods to successfully produce a detonation wave: direct ignition or self-ignition. Direct ignition requires an ignition source with enough energy to directly produce a shock wave that ignites the mixture behind it, this amount of energy is beyond the capability of conventional ignition systems, including most plasma-based ignition sources. Self-ignition occurs when a deflagration wave is formed in a confined volume such that pressure waves produced in the flame front are able to propagate upstream and coalesce into a shock wave in the unburned gas mixture ahead of the deflagration wave. Once the shock is formed, it ignites the mixture directly behind it and is then sustained by fast heat release in the reaction zone, thus becoming self-sustaining [18]. This method of initiation is by far the most common in PDE engines.

For self-ignition, the combustion process consists of three basic steps: ignition (kernel generation, kernel growth, and self-sustaining deflagration wave propagation), deflagration-to-detonation transition (DDT), and detonation wave propagation. The goal of the present study is to quantify the benefits of using a nanosecond-pulsed non-equilibrium plasma discharge in place of the standard arc discharge for ignition. For this purpose, a nanosecond-pulsed power source (FID GmbH – FPG 30-50MC4) provides pulses of up to 40 kV peak voltage for a duration of 20 ns (~4 ns rise and fall time, 12 ns at peak voltage), with a repetition frequency of up to 40 kHz. Due to the short discharge time scale, the plasma is less likely to equilibrate into an arc discharge. In an arc discharge, the electronic, vibrational, rotational, and translational temperatures of the gas are all equilibrated and can be related by the Boltzmann distribution. A standard spark ignition device, such as the Multiple Spark Discharge (MSD) ignition system used as a benchmark in this study, creates an arc discharge that initiates combustion by raising the translational gas temperature to the point where radical chain branching reactions dominate the system and the reactions proceed exponentially faster than at room temperature. Instead, in a non-equilibrium plasma discharge, the discharge energy is largely channeled into the electronic energy states of the gas molecules, and these electronically excited molecules must undergo many collisions before the energy can be equilibrated over the other energy states. This collision process with electronically excited species may open up different reaction pathways for the ignition process to proceed instead of the standard reactions happening in hot gases [17,19]. For example, in a non-equilibrium discharge there may be electron-impact dissociation reactions, low activation energy reactions with electronically excited species, and reactions with ionized molecules.

Therefore, the application of the high-frequency nanosecond-pulsed discharge for ignition can provide two important benefits: non-equilibrium excitation for ignition enhancement and high pulse repetition rates for coupling to the reactive mixture. The aim of this study is to see if this non-equilibrium high frequency discharge can accelerate ignition in PDE engines as compared to standard spark discharges, and also to identify the governing parameters (pulse voltage, frequency, and total number of pulses) which most greatly enhance the ignition process. Toward this end, Schlieren imaging of ignition events in a flow tube were recorded, and the PDE engine was fired while monitoring ignition time and wave speed throughout the detonation process.

3.2 PDE Engine and Experimental Setup

The PDE facility used in this research is located at the Air Force Research Laboratory (AFRL) at Wright-Patterson Air Force Base (WPAFB) and has been described previously in detail [20], so is only briefly discussed here. A General Motors Quad-4 Dual Overhead Cam (DOHC) 4-cylinder engine head is mounted to a thrust stand, and in place of the cylinder and piston assemblies, two steel detonation tubes are bolted to the engine head. The remaining two cylinder positions are left unused. For these experiments, the detonation tubes are 73" in length with 2.067" inner diameter. One tube is fitted with a Shchelkin spiral to enhance turbulence generation, the length of which is 3' for ethylene experiments and 4' for aviation gasoline (avgas) experiments. The other tube is a "dummy tube" and is fired along with the detonation tube to provide a more even distribution of fuel/air mixture from cycle to cycle by reducing mass build-up time in the intake manifold. This tube is fired 360° out of phase with the detonation tube. An image of the engine outfitted for detonation testing is show in Figure 9. For the Schlieren experiments, a 103" long steel tube fitted with a 36" long, 2" x 2" square polycarbonate test section is used in place of the instrumented detonation tube.

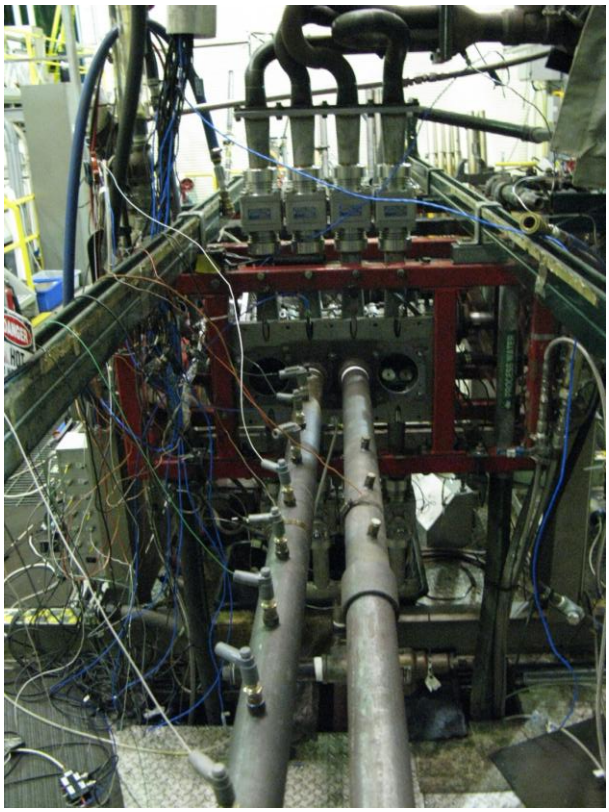

Figure 9 PDE Engine facility

The PDE diagnostic system consists of a number of sensors for monitoring the progress of the ignition event and subsequent detonation wave propagation. To understand the value of these sensors, a short description of the processes involved is necessary. The PDE works on a

three-phase (fill, fire, and purge) cycle. The first stage of the cycle consists of filling the detonation tube with premixed flammable gases through the two intake valves of the engine head. The mixing takes place just upstream of the intake manifold in a heated chamber and is well-mixed in the intake manifold before being injected into the detonation tube. Once the tube has been filled with a charge equal to the total volume of the tube, both the intake and exhaust valves are shut and the firing stage can begin. The firing process is outlined in Figure 10, and proceeds as follows: the first step of the firing stage is a user determined "ignition delay", after which the ignition device is fired. There is then some "ignition time" when the kernel develops into a self-propagation deflagration wave. Once the deflagration wave is established, it will transition into a detonation wave some distance down the tube. The time between when ignition is established and when the deflagration wave transitions into a detonation wave (DDT) is called the "DDT time". The distance down the detonation tube at which DDT is completed is called the "DDT distance." In the final step of the firing phase, the detonation wave propagates through the detonation tube and is exhausted into the exhaust tunnel of the test cell, producing thrust. A half-tube fill of fresh air is then pumped through the exhaust valves of the engine to clear the burned gas, and the process then starts over. All tests were conducted at an engine cycle rate of 10 Hz [21].

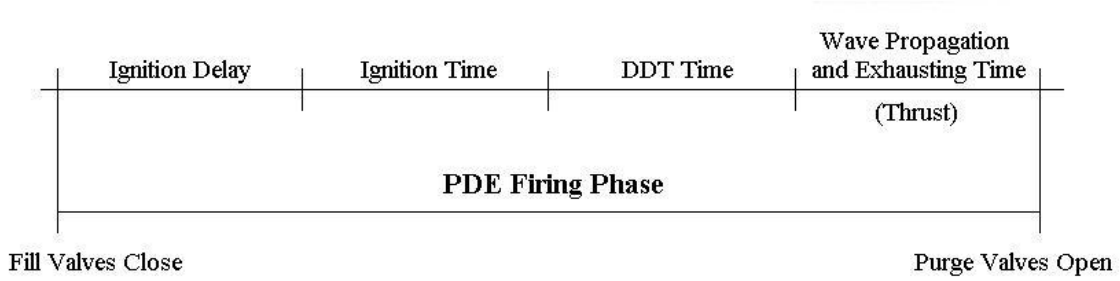

Figure 10 Sequence of events in PDE testing

The PDE diagnostics setup consists of a pressure transducer, or PCB, to monitor pressure in the engine head, an optical sensor for measuring chemiluminescence of excited OH radicals (OH*) during ignition to supplement the PCB measurements, and nine ion probes located at equal intervals of 6" along the detonation tube starting 10 1/8" from the engine head. The PCB outputs a voltage signal proportional to the change in pressure, and the ignition time is determined when the signal from this sensor reaches a slope of 5V/second. The OH sensor also measures ignition time and ignition from this sensor is determined when the signal is greater than two standard deviations above the mean. Depending on the equivalence ratio, there is always some difference between the PCB determined ignition and the OH* determined ignition. For the purpose of consistency, the PCB results will be used exclusively for this work.

The nine ion probes are essentially spark plugs with a small voltage applied across the gap which is not capable of causing breakdown in the gas. When a combustion wave passes by an ion probe, the resistance of the gas between the electrodes is reduced due to ions present in the flame front, producing a drop in the voltage signal. Thus, the position of the combustion wave can be monitored by the ion probes, and by dividing the distance between two probes by the time it takes for the combustion wave to traverse that distance, the wave speed can be calculated. This calculated wave speed is assumed to occur at the midpoint between the two

probes used to make the calculation. When two consecutive wave speed measurements result in the same value, this speed is determined to be the C-J velocity. To determine how far down the tube the combustion wave reaches the C-J velocity, the wave speed is linearly interpolated between the measurements just before and just after the C-J velocity is reached, and the distance at which the C-J velocity is first achieved is the DDT distance. The DDT time is determined by calculating the time when the wave passes through the point determined to be the DDT distance.

3.3 Nanosecond-Pulsed Ignition System

Both the nanosecond pulsed power supply and a standard spark power supply (multi-spark discharge or MSD) were used in this study. The same non-resistive spark plug and cable were used in all experiments. The spark plug was custom machined from an Autolite Racing AR3911 non-resistive spark plug. The ground strap was removed and replaced with a sharpened steel electrode. In addition, the high voltage center electrode was sharpened to a point to produce a point-to-point configuration. The gap was fixed at 1.4 mm, which was found to be the maximum gap permissible to ensure the discharge occurred only between the two pointed electrodes and not from the center electrode to the metal edge of the spark plug. The voltage and current traces were measured by a LeCroy high voltage probe (PPE20KV) and a Pearson Coil (Model 6585), respectively. A sample trace of these two signals for the nanosecond pulsed power supply is provided in Figure 11. The total energy was computed by integrating the product of these measurements (electrical power) over the duration of the discharge and subsequent reflections. A sample trace of total energy deposited per pulse as a function of time is provided in Figure 12.

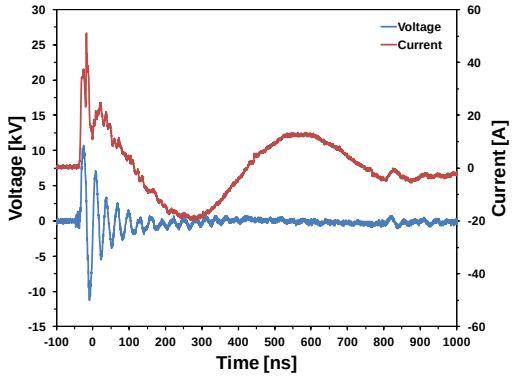

Figure 11: Voltage a current trace for a single pulse of the nanosecond ignition device. Plasma frequency = 40 kHz, φ = 0.9

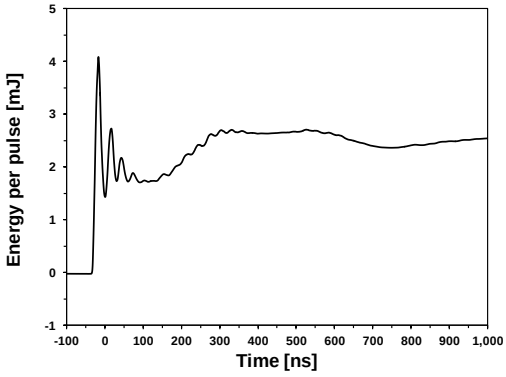

Figure 12: Calculated total energy input for a single pulse of the nanosecond ignition device. Plasma frequency = 40 kHz, φ = 0.9

The nanosecond power supply allows the capability of varying the pulse peak voltage up to 40 kV and continuous pulse frequency up to 40 kHz. The measured peak voltage was 10 kV and measured peak current was 30 A for the experiments presented herein. For this study, bursts of pulses were produced and the effect of pulse number, voltage, and frequency were investigated in the range of 1-5 mJ per pulse for 1-20 pulses in the PDE and up to 100 pulses in the Schlieren tube, covering a range of frequencies from 869 to 40,000 Hz and from the 1-10 kV peak voltage. The multi-spark discharge (MSD) is an aftermarket automotive capacitative-charge

spark ignition device, part number 6215. It produces a series of sparks (generally 3 for the current set of experiments) at a fixed rate of 869 Hz (1.15 ms between sparks). The MSD power source is generally coupled with a resistive cable and spark plug, however, in these experiments the resistive cable and spark plug were replaced by the same non-resistive ones used for the nanosecond power supply. The voltage increased to a peak of 6.5 kV in about 5 μs and after breakdown produced a peak current of 15 A for a power pulse of about 1 μs with a current pulse continuing for 50 μs thereafter [22]. The power supply energy is reported to provide between 105 and 115 mJ, however, values between 5-10 mJ were coupled into the gas, as measured in these experiments.

3.4 Schlieren Imaging

The Schlieren setup consisted of an LED light source, collimating mirrors, a razor edge, and a Phantom v711 high speed CMOS camera. The light emitted from the LED source is collimated by the mirrors (100" focal length) and sent through the polycarbonate walls of the Schlieren test section. A mirror setup identical to the collimating mirrors focuses the light onto the CMOS chip of the camera after passing through the test section. Half of this light is cut off by the razor edge, thus producing an image with light and dark regions which correspond to density gradients in the flow. Images are collected just before the ignition event and extend until the combustion wave has fully propagated out of the view of the camera. The frame rate used in all imaging is 100,000 fps. To process these images, the frames just before the ignition event were averaged, thus providing a "background" image. The images of the ignition event and the subsequent flame propagation were divided by this background image, providing a contrast which produced a clear view of the combustion wave front. Artificial coloring was then applied for easier visual identification of the flame front. Due to oil seeding into the air flow for the engine valve lubrication, the Schlieren images degraded between window cleanings, however it was still possible to follow the kernel growth and development stages for different ignition conditions using both ethylene/air and methane/air mixtures.

The effects of total energy input, discharge frequency, and discharge voltage were each studied by independently varying the parameters. Each condition was run for five ignition events and the plotted data is the average of these. The results of the PDE engine testing were collected for the following ranges:

Fuel	Equivalence Ratio	Energy/pulse	Pulse frequency	Number of pulses
Ethylene	0.7-1.8	1-5 mJ	869-40,000 Hz	2-10
Avgas	0.9-1.4	1-5 mJ	869-40,000 Hz	2-20

Table 2 PDE engine testing conditions

For varying equivalence ratios, the nanosecond pulse power supply was held constant at its peak value (corresponding to 3-5 mJ per pulse) and peak frequency of 40 kHz while the

number of pulses was varied from 2-20 for avgas and 2-10 for ethylene at each equivalence ratio. The results are plotted in Figures 13 and 14, as well as the MSD results as a benchmark.

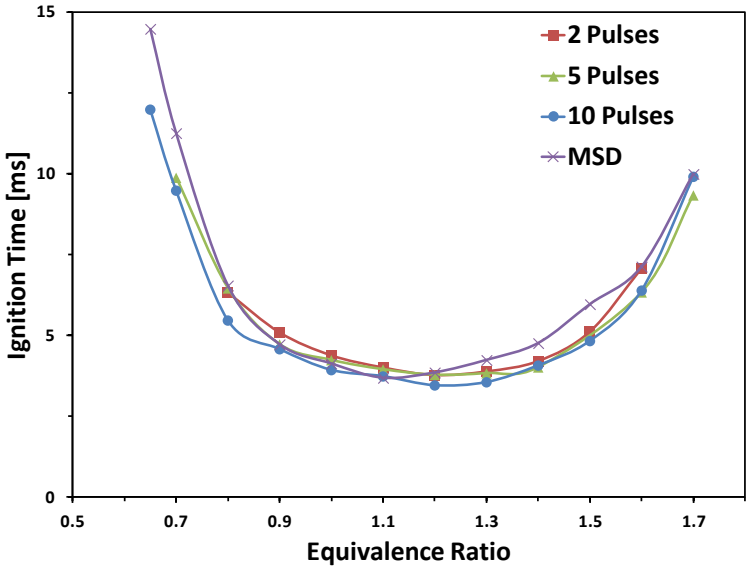

Figure 13: Ethylene/Air at 3-5 mJ per pulse, 40 kHz for the nanosecond plasma.

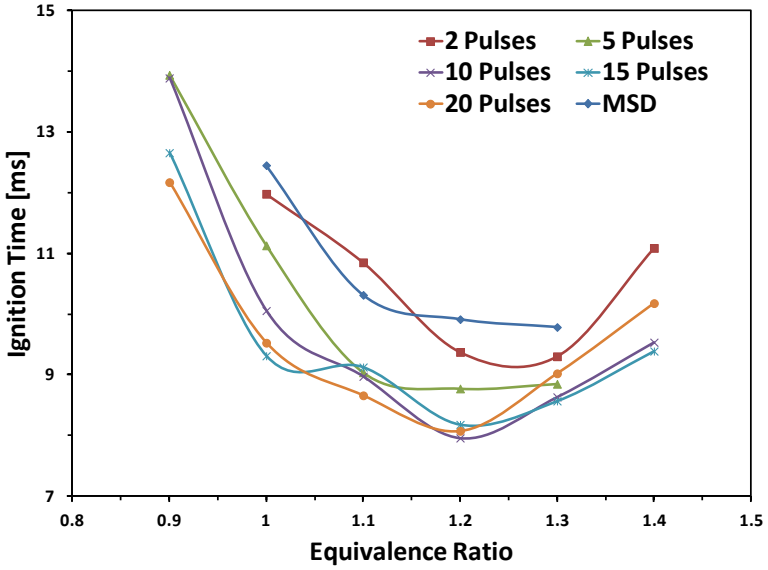

Figure 14: Avgas/Air at 3-5 mJ per pulse, 40 kHz for the nanosecond plasma.

For both ethylene and avgas, the nanosecond pulse device produces shorter ignition times for most equivalence ratios when more than two pulses were supplied. Two pulses contained about the same amount of energy as a single spark from the MSD ignition source, and so it is not surprising that two high frequency pulses produced equivalent ignition times as the MSD. In the

case of avgas, the nanosecond pulser could achieve ignition at leaner and richer equivalence ratios than the MSD igniter, as indicated by the lack of ignition data for the MSD at the lean/rich limits of the data set. The above results are plotted as percent decrease in ignition time in Figures 15 and 16, and only represent cases were both ignition devices were functioning.

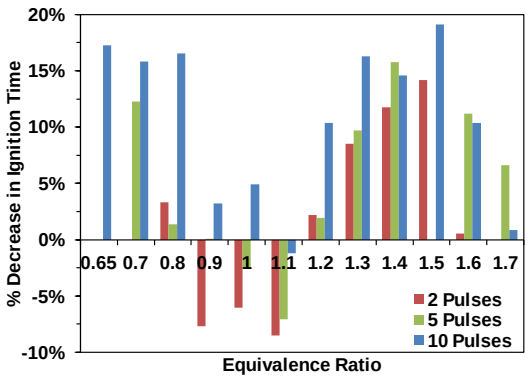

Figure 15: Percent decrease in ignition time for ethylene/air using the nanosecond pulser at 3-5 mJ per pulse, 40 kHz

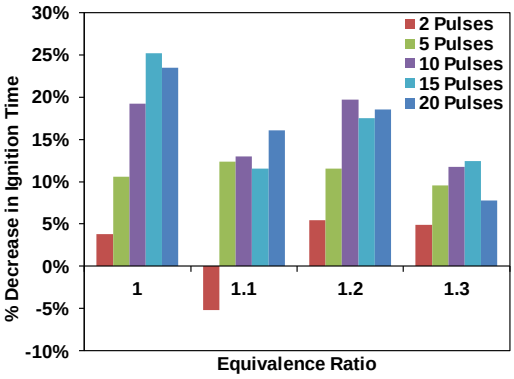

Figure 16: Percent decrease in ignition time for avgas/air using the nanosecond pulser at 3-5 mJ per pulse, 40 kHz

In the case of ethylene, the ignition time enhancement of the nanosecond pulser is less obvious at near stoichiometric conditions, and is often even slower than the spark ignition, but near the lean limit it is clear that 10 nanosecond pulses produces shorter ignition time than the MSD. In the case of avgas, ignition is almost always faster using the pulser for all equivalence ratios, and the percent decrease in ignition time is greater than in the ethylene case. It can be inferred from these trends that when the ignition time is longer, the nanosecond pulser has a greater effect on the ignition time. If the ignition time is longer, the nanosecond pulser can add more energy to the ignition kernel before it expands away from the spark gap region. In the case of stoichiometric ethylene, the minimum ignition energy is very low, while the reaction rate is very fast, thus not many pulses of the plasma can couple into the kernel before the flame front has left the region. Thus the plasma igniter has no significant advantage over the standard spark. In fact, because more energy is coupled in to one MSD spark than in one plasma pulse, it makes sense that for φ=0.9-1.1 the MSD igniter is faster than the plasma igniter, since initially the spark ignition system has a faster energy deposition rate.

To explore the effects of plasma parameters, two equivalence ratios for each ethylene and avgas were selected to be held constant while the plasma parameters were changed. For ethylene, φ=0.8 and φ=1.0 were selected; while for avgas, φ=1.0 and φ=1.1 were selected. This provided an idea of how longer or shorter characteristic fuel ignition delays could be altered by the plasma igniter. The results of these tests are plotted in Figures 17-20.

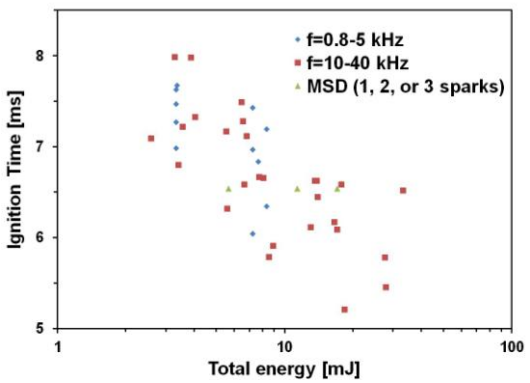

Figure 17: Ethylene/air, φ=0.8.

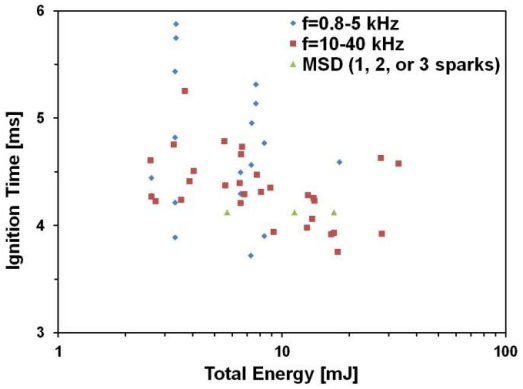

Figure 18: Ethylene/air, φ=1.0.

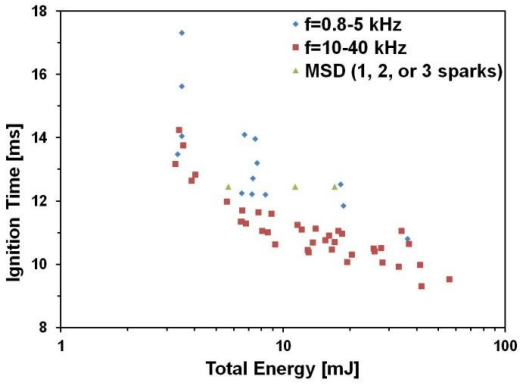

Figure 19: Avgas/air, φ=1.0.

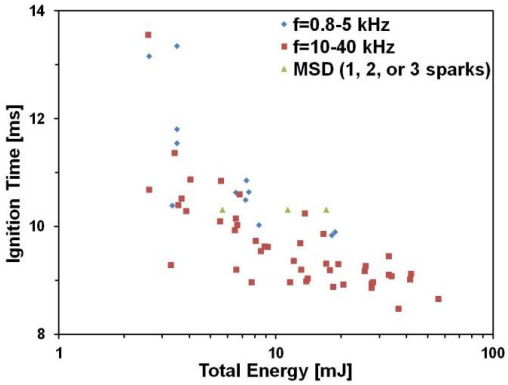

Figure 20: Avgas/air, φ=1.1.

Two trends emerged in the data. The first, and most obvious, is the decrease in ignition time with increase in total energy (number of pulses multiplied by energy per pulse). The trend is for the most part not apparent in the stoichiometric ethylene/air experiments. As mentioned earlier, this is because there is not much time to couple additional energy into the kernel before it has left the region of the spark plug. The second trend is the decrease of ignition time with increased pulse frequency. This trend is significantly more apparent in the avgas data, which has in general about twice the ignition time as ethylene. Under about 10 kHz, there is a noticeable drop off in ignition time for the same total energy input, particularly in the avgas data. Two plausible reasons for this trend emerge. The first is that more of the total energy can get coupled into the ignition kernel before it moves away from the spark region if the energy is coupled into the gas faster. The second reason is that, at high frequency, left over electrons and ions from previous pulses of the ignition device are still available when the next pulse arrives. This reduces the amount of energy spent ionizing the gas, and allows more of the energy to be spent accelerating free electrons and ions which can then react with the fuel, oxygen, and nitrogen molecules and create radicals and excited species which kinetically increase the reaction speed. The two effects may couple with each other due to the presence of electrons and ions generally present in flames. Further evidence of this trend will be provided in voltage and current traces of the entire pulse train, as well as high speed imaging of the discharge.

A visual investigation of the ignition process further confirms the trends seen in the PDE data, demonstrated in Figure 21. The Schlieren data has been artificially colored to make the flame front more obvious. Similar conditions as for the PDE data set were taken for the Schlieren experiments. Instead of avgas, methane was used to demonstrate the decrease in ignition time for a fuel with long characteristic ignition times. This is because the heat required to keep avgas from condensing on the walls of the tube would weaken the polycarbonate windows. Although a large amount of data is available, only some of the most revealing images are presented herein.

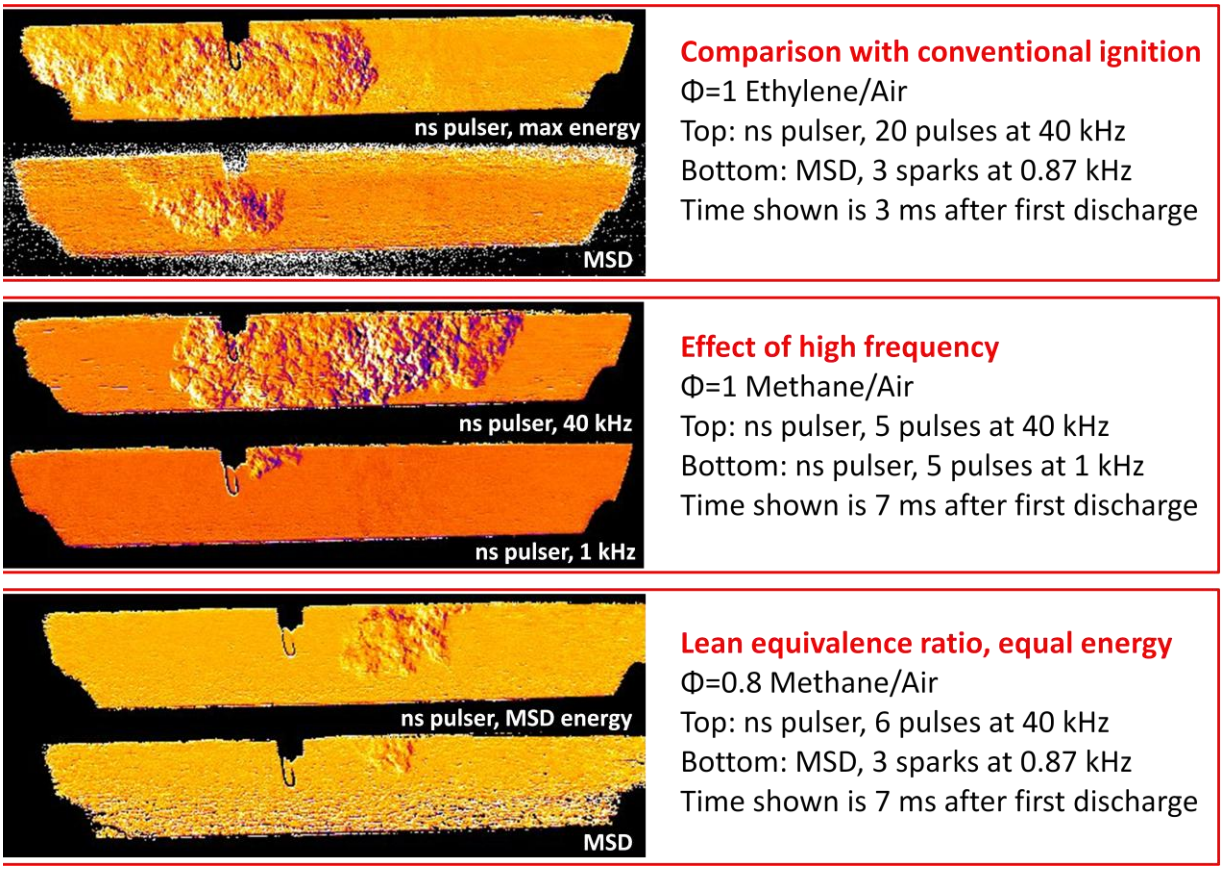

Figure 21 Schlieren Imaging

The top images show a faster development of the ignition event using the nanosecond pulser as compared to the MSD. In the PDE data, it was often difficult to detect any decrease in ignition time using the plasma igniter for stoichiometric ethylene/air ignition. However, it is clear that the kernel develops into a self-propagating flame front faster for the plasma igniter in the images, which are capable of revealing much finer detail in the ignition process than the head mounted PCB sensor. The second image shows the effect of plasma frequency for the same total energy input. This presents the dramatic benefit of the high frequency pulsed plasma. The last images are a comparison of the MSD and the nanosecond pulser when the total energy input is roughly equivalent. In this event, the MSD ignition kernel eventually extinguishes, while the plasma ignited kernel goes on to become a self-propagating flame. This again demonstrates the benefit of high frequency energy addition as compared to lower frequency, higher single pulse energy discharges.

4. Conclusion

A microwave-assisted spark plug and a nano-second pulsed spark plug were developed to enhance ignition and combustion efficiency for a small scale internal combustion engine and a pulse detonation engine. An engine test platform was developed to measure engine torque and pressure quantitatively. The experimental results demonstrated the superior characteristics of engine performance using these new ignition systems. The experimental tests of the microwave-enhanced spark ignition for two small scale engines (Fuji BF-34EI 34 cc engine) showed that the microwave-assisted ignition system was able to broaden the engine lean operational limits by more than 20%. Moreover, a significant increase of the maximum engine pressure was observed. The nanosecond-pulsed device was tested in collaboration with researchers at the AFRL in a pulse detonation engine at Wright-Paterson AFB. It was also found that the lean limit could be extended by the non-equilibrium plasma ignition system as compared to the conventional spark ignitor. Furthermore, the ignition time, which limits engine performance, could be reduced by up to 25%. The above results demonstrated clearly that plasma assisted ignition is a promising technique to enhance ignition of propulsion systems.

Acknowledgement: The PI would like to express his sincere thanks to the support and help of Drs. Ryoji Tsuruoka and Yuji Ikeda from Imaging Engineering Inc. in establishing the microwave assisted ignition system. The PI also thanks Drs. Fred Schauer and Timothy Ombrello at AFRL for many technical advices and collaboration.

5. References

1. Ju, Yiguang, and Kaoru Maruta. "Microscale combustion: Technology development and fundamental research." *Progress in Energy and Combustion Science* 37.6 (2011): 669-715.
2. Fernandez-Pello A. Carlos, “Micropower generation using combustion: issues and approaches”, *Proc. Combust. Inst.*, Vol. 29, 2002, p.883-899.

3. Ming-Hsun Wu, Richard A. Yetter and Vigor Yang, "Development and Characterization of Ceramic Micro Chemical Propulsion and Combustion Systems", *The 46st AIAA Aerospace Sciences Meeting and Exhibit*, AIAA Paper 2008-0966, Reno, NV, U.S.A., 2008.
4. Daou, J., and Matalon, M. (2002) "Influence of conductive heat-losses on the propagation of premixed flames in channels", *Combust. Flame* 128, p.321.
5. B. Lewis G. Von Elbe, *Combustion Flames and Explosive of Gases*, Academic Press, New York, 1961
6. Y. Ju and B. Xu, "Theoretical and experimental studies on mesoscale flame propagation and extinction," Proceedings of the Combustion Institute 30(2005), 2445–2453.
7. Daou, J., and Matalon, M. (2002) Influence of conductive heat-losses on the propagation of premixed flames in channels, Combust. Flame 128, p.321.
8. Andrey Nikipelov, Aleksandr Rakitin, Andrei Starikovskii, Low-Temperature Plasma Chemistry and Plasma Assisted Partial Oxidation, AIAA-2009-224, 47th AIAA Aerospace Sciences Meeting, Orlando, Florida, Jan. 5-8, 2009.
9. Timothy Ombrello, Sang Hee Won, Yiguang Ju, and Skip Williams, OH Lifted Flame Speed Enhancement by Plasma Excitation of Oxygen, AIAA-2009-689, 47th AIAA Aerospace Sciences Meeting, Orlando, Florida, Jan. 5-8, 2009.
10. Anatoly Klimov, Valentin Bityurin, A Grigorenko, V Kutlaliev, I Moralev, B Tolkunov, A Tsymbal, Plasma Assisted Combustion of Heterogeneous Fuel in High-Speed Airflow, AIAA-2009-1411, 47th AIAA Aerospace Sciences Meeting, Orlando, Florida, Jan. 5-8, 2009.
11. Ashim Dutta, Inchul Choi, M Uddi, Evgeny Mintusov, A Erofeev, Z Yin, Walter Lempert, Igor Adamovich, Cavity Flow Ignition and Flameholdingin Ethylene-Air by a Repetively Pulsed Nanosecond Discharge, AIAA-2009-821, 47th AIAA Aerospace Sciences Meeting, Orlando, Florida, Jan. 5-8, 2009.
12. Emanuel Stockman, James Michael, Alex Fuller, Sohail Zaidi, and Richard Miles, Toward High Q, Evanescent Coupled Microwave Controlled Combustion, *AIAA-2009-491* 47th AIAA Aerospace Sciences Meeting, Orlando, Florida, Jan. 5-8, 2009.
13. Wenting Sun, Mruthunjaya Uddi, Timothy Ombrello, Sang Hee Won, Cambpell Carter, Yiguang Ju, Effects of Non-Equilibrium Plasma Discharge on Counterflow Diffusion Flame Extinction, Proc. Combustion Institute, Vol.33, in press, 2010.
14. M. Uddi, N. Jiang, E. Mintusov, I.V. Adamovich, W.R. Lempert, Proc. Combust. Inst. 32 (2009) 929-936.
15. Ikeda, Y., Nishiyama, A., and Kaneko, M., "Microwave Enhanced Ignition Process for Fuel Mixtures at Elevated Pressure of 1 MPa," AIAA-2009-223587.
16. ElSabbagh, M., Kado, S., Ikeda, Y., Sasaki, K., "Measurements of Rotational Temperature and Density of Molecular Nitrogen in Spark-Plug Assisted Atmospheric-pressure Microwave Discharges by Rotational Raman Scattering." *Japanese Journal of Applied Physics*, Vol. 50, 2011, doi:076101.
17. Pancheshnyi, S.V., Lacoste, D.A., Bourdon, A., Laux, C.O. "Ignition of Propane-Air Mixtures by a Repetitively Pulsed Nanosecond Discharge" *IEEE Transactions on Plasma Science*, Vol. 34, No. 6 (2006).
18. Glassman, I. and Yetter, R.A. *Combustion.* Elsevier, Inc (2008).
19. Starikovskii, A.Yu., Anikin, N. B., Kosarev, I. N., Mintoussov, E. I., Starikovskaia, S. M., and Zhukov, V. P.. "Plasma-assisted combustion" *Pure Appl. Chem.*, Vol. 78, No. 6, pp. 1265–1298 (2006).

20. Schauer, F., J. Stutrud, and R. Bradley. Detonation initiation studies and performance results for pulsed detonation engine applications. *AIAA Paper 2001-1129* in 39th AIAA Aerospace Sciences Meeting and Exhibit,. 2001. Reno, Nevada.
21. Naples, A., Yu, S.T., Hoke, J., Busby, K., Schauer, F. "Pressure Scaling Effects on Ignition and Detonation Initiation in a Pulse Detonation Engine" *47th AIAA Aerospace Sciences Meeting Including The New Horizons Forum and Aerospace Exposition 5 - 8 January 2009, Orlando, Florida*
22. Busby, K., et al. Effects of Corona, Spark and Surface Discharges on Ignition Delay and Deflagration-to-Detonation Times in Pulsed Detonation Engines. *AIAA 2007-1028* in 45th AIAA Aerospace Sciences Meeting and Exhibit. 2007: AIAA 2007-1028.

6. Publications

1. Tropina, A.A., Uddi, M., and Ju, Y.On the effect of nonequilibrium plasma on the minimum ignition energy - Part 1: Discharge model, *IEEE Transactions on Plasma Science* 39 (2011), 615 – 623.

2. Lefkowitz, Joseph K., Ju, Yiguang, Tsuruoka, Ryoji, Ikeda, Yuji, "A Studies of Plasma-Assisted Ignition in a Small Internal Combustion Engine" *50th AIAA Aerospace Sciences Meeting*, 9-12 Jan. 2012, Nashville, Tennessee.

7. Personnel

Investigators			
Yiguang Ju	PI	Princeton University	yju@princeton.edu
Fredrick L. Dryer	Co-I	Princeton University	fldryer@princeton.edu
Professional Staff			
Sang Hee Won	Research Associate	Princeton University	2010-2011

Graduate Students			
Joseph K. Lefkowitz	Doctoral Student	Princeton University	2010-2012
Wenting Sun	Doctoral Student	Princeton University	2010-2012
Mruthunjaya Uddi	Doctoral Student	Princeton University	2010-2012
Undergraduate Students			
Matthew K. Chu Cheong	Summer Student/ Independent Research	Princeton University	2011-2012
Jonathon E. Surany	Independent Research	Princeton University	2011